Int. J. Electron. Commun. (AEÜ) 78 (2017) 141–156

Contents lists available at ScienceDirect

International Journal of Electronics and Communications (AEÜ)

journal homepage: www.elsevier.com/locate/aeue

Regular paper

Real time implementation of fractional order PID controllers for a magnetic levitation plant

Subrat Kumar Swain [a,*], Debdoot Sain [b], Sudhansu Kumar Mishra [a], Subhojit Ghosh [c]

[a] Dept. of Electrical and Electronics Engineering, Birla Institute of Technology, Mesra, Ranchi 835215, India
[b] Dept. of Electrical Engineering, Indian Institute of Technology, Kharagpur 721302, India
[c] Dept. of Electrical Engineering, National Institute of Technology, Raipur 492010, India

ARTICLE INFO

Article history:
Received 24 December 2016
Accepted 19 May 2017

Keywords:
Fractional calculus
Fractional order PID
Integer order PID
Maglev system
Robustness

ABSTRACT

Fractional calculus has been a topic of great interest for the last few decades. The applications of fractional calculus can be found in the area of viscoelastic and chaotic systems, whose dynamics is expressed in the form of fractional differential equations. The ongoing research work is based on the design of 1-Degree of Freedom (1-DOF) and 2-Degrees of Freedom (2-DOF) Fractional Order PID (FOPID) controllers for a Magnetic levitation (Maglev) plant and the performance has been compared with that of 1-DOF and 2-DOF Integer Order PID (IOPID) controllers in both simulation and real time. The Degree of Freedom (DOF) represents the number of feed-forward control loops in a closed loop system. A 2-DOF controller configuration comprises of a serial compensator and a feed-forward compensator in a closed loop structure. An FOPID controller has a structure similar to that of a conventional IOPID controller, except that its derivative and integral orders are fractional numbers. The design of such a controller requires the determination of five parameters: K_p, K_i, K_d, α and β, where α and β are the derivative and integral orders of the FOPID controller. The controller design problem has been framed as an optimization problem, in which the cost function is formulated from the characteristic equation of the closed loop system at dominant poles that are identified from the given performance specifications. The closed loop response shows that the proposed2-DOF FOPID controller exhibits superior response and robustness with respect to its integer order counterpart.

1. Introduction

Fractional order calculus has been a topic of immense interest for the last few decades. The concept of fractional calculus and its extension in the design of fractional order PID control was first proposed by Podlubny [1]. The application of fractional calculus in electro-chemistry, biological systems, material science, viscoelastic and chaotic systems has been widely explored in literature [2,3], and [4]. Realization of fractional order systems in digital and hardware domain can be explored in [5,6], and [7]. A novel design method for a fractional order controller which can be considered as a special case of fractional PID for fractional order systems with time delay as the desired transfer function response, has been described in the literature [8]. In [9], the author(s) discusses the design of a FOPID controller whose parameters are the solution of a constrained min-max optimization problem. The objective function involves minimization of the maximum sensitivity subjected to the various constraints among which the most important one is the isodamping condition. The stabilizability criteria for unstable time delay processes by fractional order controllers has been discussed in [10,11] whereas in [12] the author(s) explore a novel methodology for the computation of stable regions from which identifying the parameters of fractional order PI and fractional order PD has been dealt with. The design of a Fractional order controller for a heat flow process modelled as an integer first-order plus time delay system is investigated through simulation and through real time experimentation [13]. The design of an extended state observer based fractional order PD controller for trajectory tracking accuracy for a novel linear motor is explored in [14]. Tuning algorithms for the design of fractional order internal model controllers for time delay processes has been described in [15]. The modelling of systems employing the concept of fractional differentiation has become extremely popular in recent times because of the availability of advanced computational

* Corresponding author.
E-mail addresses: swain.subrat01@gmail.com (S.K. Swain), hiidebdoot@gmail.com (D. Sain), sudhansu.nit@gmail.com (S.K. Mishra), sghosh.ele@nitrr.ac.in (S. Ghosh).

http://dx.doi.org/10.1016/j.aeue.2017.05.029
1434-8411/

packages that has simplified the simulation and implementation of these systems with adequate precision.

Like integer order controllers, the design of a fractional order PID(FOPID) controller involves the tuning of its parameters, so as to meet the desired specifications. The application of optimisation methods for the tuning of FOPID parameters can be studied in [16,17] and [18]. The tuning of parameters for FOPID controllers by the Ziegler-Nichols method is reported in [19]. In [20] a novel method for tuning FOPID parameters based on minimizing the integral absolute error with a constraint on the maximum sensitivity has been described. The authors in [21], proposed a method to design a robust fractional order controller for unstable plants having one unstable pole based on the quantitative feedback theory using particle swarm optimisation. The design of a PID controller for fractional order systems with time delays is discussed in [22–24] and [25]. The authors in [26], proposed a method to determine FOPID parameters for an automatic voltage regulator using particle swarm optimisation. The design of FOPID controllers for a class of fractional order plants using the dominant pole placement method is reported in [27,28]. There are several other methods of tuning the FOPID controller that can be explored in [29–33] and [34]. The design of 1-DOF and 2-DOF IOPID controllers for a benchmark control problem of Magnetic Levitation System plant using pole placement method is reported in [35]. A novel method for the analog implementation of the fractional order controller whose transfer function is obtained by the Inverse-Follow-the-Leader-Feedback topology is reported in [36]. The authors in paper [37] proposed an electrical analog of a fractional order mechanical impedance model representing the human respiratory system using approximated fractional order capacitors and inductors. One of the limitations that can be explored in the existing literature including the results reported in [27,28], and [35] is the need for a more efficient modified fractional order controller, apart from the conventional 1-DOF FOPID controller. The Degree of Freedom (DOF) represents the number of feed-forward control loops in a closed loop system. A 2-DOF controller configuration comprises of a serial compensator and a feed-forward compensator in a closed loop structure. The novelty of the work concerns the application of the dominant pole placement approach for the design of 1-DOF, 2-DOF IOPID and FOPID controller for an inherently nonlinear plant i.e. magnetic levitation, with its validation and performance analysis using both simulations and hardware implementation in real time. The present work explores the potential of the 2-DOF FOPID controller over other conventional integer order PID controller configurations in generating superior frequency domain specifications satisfying the iso damping property using both simulations and hardware experiment. The hardware implementation allows validation of the controller performance for real time environment. The control problem was addressed by framing up an objective function formulated by substituting either of the dominant poles in the characteristic equation and equating it to zero. The controller parameters were obtained after optimizing the objective function using the nonlinear interior point optimization technique in MATLAB. The proposed methodology was then validated on an experimental magnetic levitation set-up provided by Feedback Instruments in the Control System Laboratory of BIT Mesra.

This paper is organised as follows. In Section 2, a brief introduction to the Maglev plant is given. In Section 3 the mathematical foundation of the fractional order controller is introduced. In Section 4, the methodology involved in the formulation of the cost function for the integer order and fractional order controllers is proposed. In Section 5, the nominal set point tracking for both 1-DOF and 2-DOFIOPID and FOPID controllers is discussed. In Section 6, the system's robustness to model uncertainties is presented. Finally, the conclusions are drawn in Section 7.

2. Maglev system

The Maglev setup (Model No. 33-210 from Feedback Instruments Ltd.) [38] serves as a simple model of practical devices whose applications can be found in Maglev trains and magnetic bearings, and which have achieved immense popularity in recent years. The magnetic levitation systems are appealing for their additional possibility of active vibration damping. This can be achieved by the implementation of various control algorithms without any modification to the mechanical parts of the whole system. The design and test of different controllers is possible through this Maglev set up in real time environment using MATLAB and Simulink.

The Maglev unit consists of a connection-interface panel along with a mechanical-electrical part. A coil is mounted on the mechanical part and an Infrared (IR) sensor is attached to it which continuously measures the position of the ball which is related to its equivalent voltage by a proportionality factor called as sensor gain (k_2). The IR sensor converts the position of the ball to its corresponding sensor voltage (x_v). The Analog to Digital (A/D) Interface converts this feedback sensor voltage (x_v) to digital output which is then compared with the reference trajectory to produce the error signal that is finally fed to the controller to produce the controlled output 'u(t)'. The output of the controller 'u(t)' is fed to the Digital to Analog (D/A) converter which generates analog controlled output that is related to the coil current in terms of a proportionality factor called as coil current gain (k_1). The flow of current in the coil produces the force generated by the magnetic field that counterbalances the gravitational pull of the ball. The mechanical, electrical unit along with connection-interface panel that assembles into a complete control system setup is provided in Fig. 1. The system parameters of the Maglev system are presented in Table 1.

The schematic diagram of the Maglev system [35] considered for this study is provided in Fig. 2

The simplest nonlinear model [36] in terms of ball position x and electromagnetic coil current i is given by

$$m\ddot{x} = mg - k\frac{i^2}{x^2} \tag{1}$$

where, m is the mass of the ball, g is gravitational constant and k depends on the coil parameters.

In absence of the control voltage, the response of non-linear Maglev plant is shown in Fig. 3

For the analysis of the model dynamics using techniques such as Bode plots, pole and zero maps, Nyquist plots, and root locus, the model has to be linearized. In order to linearize the nonlinear Maglev plant, the calculation of an equilibrium point is mandatory. The equilibrium point of the current and position is calculated by equating $\ddot{x} = 0$ and is found to be 0.8A and 0.009 m (-1.5 V, when expressed in volts) respectively.

The nonlinear system (1) can be linearized to

$$\Delta\ddot{x} = -\left(\left.\frac{\partial f(i,x)}{di}\right|_{i_0,x_0}\Delta i + \left.\frac{\partial f(i,x)}{dx}\right|_{i_0,x_0}\Delta x\right) \tag{2}$$

where, Δx and Δi are the small deviation from the equilibrium point x_0 and i_0 respectively.

Evaluating partial derivatives and taking Laplace transform on both side of Eq. (2), the transfer function can be obtained as

$$\frac{\Delta x}{\Delta i} = \frac{-k_i}{s^2 - k_x} \tag{3}$$

where, $k_i = \frac{2g}{i_0}$ and $k_x = \frac{2g}{x_0}$ [35]

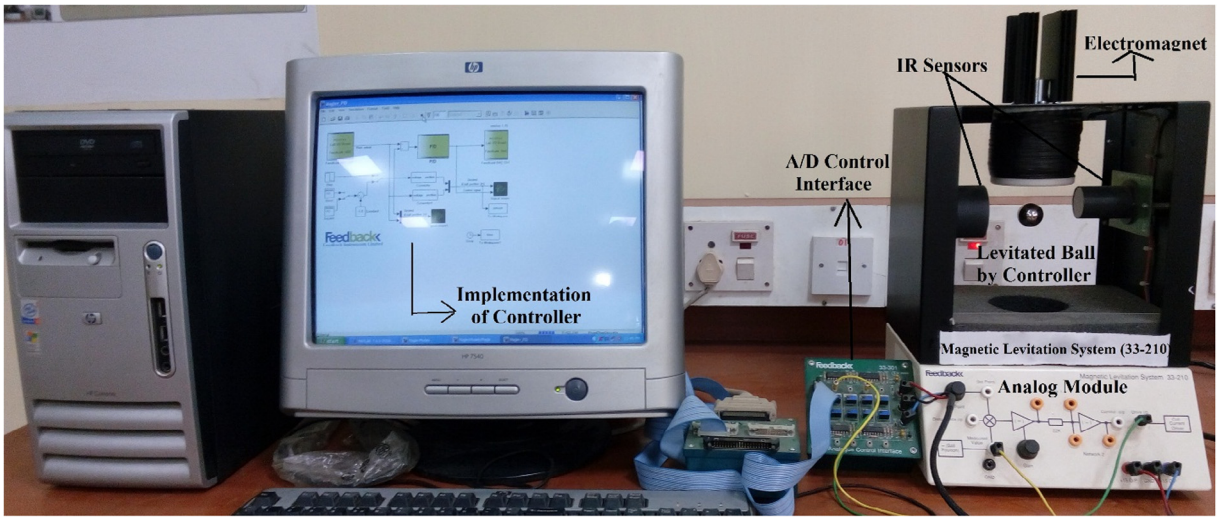

Fig. 1. Maglev control system.

Table 1
The system parameters of the Maglev system [35].

Parameter	Notation	Value
Mass of the steel ball	m	0.02 kg
Acceleration due to gravity	g	9.81 m/s^2
Equilibrium value of current	i_0	0.8 A
Equilibrium value of position	x_0	0.009 m
Control voltage to coil current gain	k_1	1.05 A/V
Sensor gain, offset	k_2, η	143.48 V/m, −2.8 V
Control voltage input level	u	±5 V
Sensor output voltage level	x_v	+1.25 V to −3.75 V

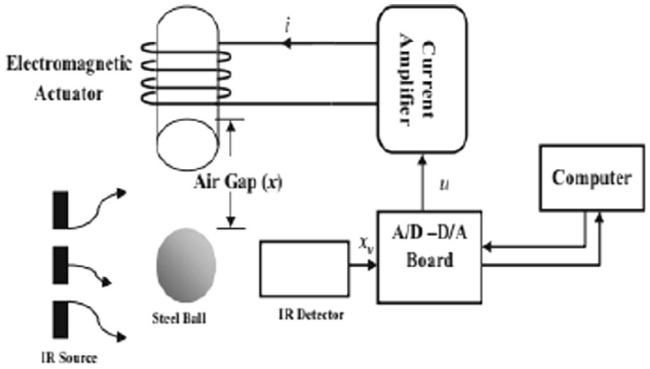

Fig. 2. Schematic diagram of Maglev system.

As x and i are proportional to x_v and u , the transfer function can be modified to the form $\frac{\Delta x_v}{\Delta u}$ [35] and is given by

$$G_P(s) = \frac{\Delta x_v}{\Delta u} = \frac{-k_1 k_2 k_i}{s^2 - k_x} \tag{4}$$

where, k_1 and k_2 are coil voltage to coil current gain and sensor voltage respectively.

With the parameters provided in Table 1, the plant transfer function becomes

$$G_P(s) = \frac{\Delta x_v}{\Delta u} = \frac{-b}{s^2 - p^2} = \frac{-3518.85}{s^2 - 2180} \tag{5}$$

The poles of the Maglev system are located at ± 46.69. Because of the presence of one pole on the right half of 's' plane, the system becomes highly unstable. To achieve a stable and controlled behaviour of the system, it becomes extremely important to design a suitable controller.

3. Fractional-order calculus

Fractional-order calculus is a branch of mathematics which deals with non-integer order derivatives and integrals. In other words, it is a generalization of the traditional calculus with a much wider applicability. The fractional calculus has been rediscovered once again in last two to three decades by the scientists and engineers, and applied in an increasing number of fields. The recent applications of fractional calculus include dynamical systems in

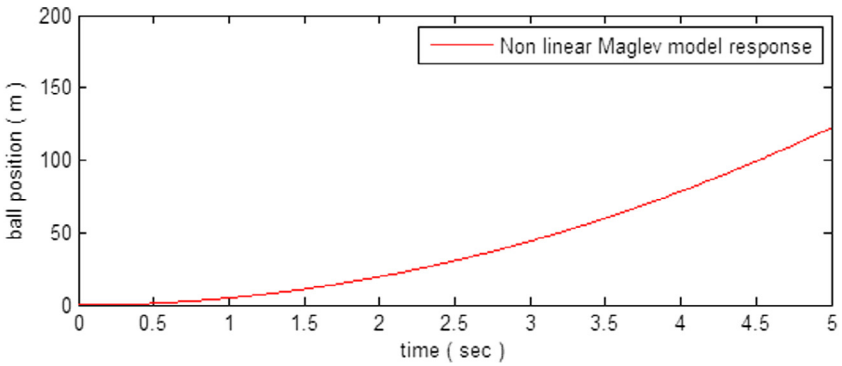

Fig. 3. Non-linear Maglev model response.

control theory, electrical circuits with fractance, generalized voltage divider, viscoelasticity, fractional-order multipoles in electromagnetism, electrochemistry, tracer in fluid flows, and model of neurons in biology [39]. The success story of fractional calculus continues with the continuous emergence of effective methods in the differentiation and integration of non-integer order equations.

3.1. Integro-differential operator

The Integro-differential operator is denoted by ${}_{a}\mathbf{D}_{t}^{\alpha}$. where a and t are the limit of operation. Depending on the value of α, this single operator can be used for both the fractional integration and differentiation. The definition of integro-differential operator is given by

$$ {}_{a}D_{t}^{\alpha} = \begin{cases} \frac{d^{\alpha}}{dt^{\alpha}} & \Re(\alpha) > 0 \\ 1 & \Re(\alpha) = 0 \\ \int_{a}^{t} (d\tau)^{-\alpha} & \Re(\alpha) < 0 \end{cases} \tag{6} $$

where, α is the order of operation. In general, $\alpha \in R$ but αcould also be a complex number [40].

3.2. Definition of fractional differintegral

In the literature of fractional calculus, there are several definitions available for fractional Differintegral. Two most famous definitions used for fractional differentiation and integration are the Grunwald-Letnikov and Reimann-Liouville definition [41].

3.2.1. Grunwald-Letnikov definition

In fractional calculus, the Grünwald–Letnikov definition is a basic extension of the backward finite difference formula for successive differentiations which allows to deal with non-integer order differentiation and integration.

According to Grunwald-Letnikov definition, the α^{th} order differintegration of a function $f(t)$ is defined as

$$ D_{t}^{\alpha} f(t) = \lim_{h \to 0} \frac{1}{h^{\alpha}} \sum_{j=0}^{\infty} (-1)^{j} \binom{\alpha}{j} f(t - jh) \tag{7} $$

where, $\binom{\alpha}{j}$ denotes the binomial coefficient and is represented as

$$ \binom{\alpha}{j} = \frac{\alpha!}{j!(\alpha - j)!} = \frac{\Gamma(\alpha + 1)}{\Gamma(j + 1)\Gamma(\alpha - j + 1)} \tag{8} $$

$\Gamma(.)$ denotes the standard Gamma function which can be represented as

$$ \Gamma(z) = \int_{0}^{\infty} e^{-u} u^{z-1} du \text{ where}, \forall z \in \mathbb{R} \tag{9} $$

For complex number, to get a finite value of the gamma function, the real part of z has to be positive. The Laplace transform of Grünwald–Letnikov fractional Differintegral is given by

$$ \int_{0}^{\infty} e^{-st} {}_{0}D_{t}^{\alpha} f(t) dt = s^{\alpha} F(s) \tag{10} $$

3.2.2. Reimann-Liouville definition

Reimann-Liouville definition is an extension of n-fold successive integration. It is widely used for finding fractional Differintegrals. The α^{th} order integration of a function $f(t)$ according to Reimann-Liouville definition is defined as

$$ {}_{a}I_{t}^{\alpha} = {}_{a}D_{t}^{-\alpha} f(t) = \frac{1}{\Gamma(-\alpha)} \int_{a}^{t} \frac{f(\tau)}{(t - \tau)^{\alpha+1}} d\tau \tag{11} $$

where, $a, \alpha \in \mathbb{R}$,a and t are the limits of operation and $\alpha < 1$.

The integer order successive differentiation of a fractional order integral that is used for defining the fractional order differentiation, can be expressed as

$$ {}_{a}D_{t}^{\alpha} f(t) = \frac{1}{\Gamma(n - \alpha)} \frac{d^{n}}{dt^{n}} \int_{a}^{t} \frac{f(\tau)}{(t - \tau)^{\alpha+1}} d\tau \text{ where}, n - 1 < \alpha < n \tag{12} $$

The Laplace transform of Reimann-Liouville fractional differintegral is

$$ \int_{0}^{\infty} e^{-st} {}_{0}D_{t}^{\alpha} f(t) dt = s^{\alpha} F(s) - \sum_{k=0}^{n-1} s^{k} {}_{0}D_{t}^{\alpha-k-1} f(t)|_{t=0} \tag{13} $$

3.3. Stability of fractional LTI system

It is known that a Linear-Time-Invariant (LTI) system is stable if all the roots of the characteristics equation lie on the left half of the complex plane. For the fractional order LTI system, the region of stability differs from the integer one. A stable fractional order system may have roots in the right half of the complex plane. In [42], it has been shown that the fractional order system (15) is stable if $|\arg(eig(A))| > q\frac{\pi}{2}$ where, $0 < q < 1$ and eig (A) represents the eigenvalue of matrix A.According to Matingon's stability theorem, the fractional transfer function $G(s) = \frac{Z(s)}{P(s)}$ is stable if and only if $|(\arg(\lambda_i)| > q\frac{\pi}{2}$, for all i, where λ_i is the i^{th} root of $P(s^q)$. The region of stability of the fractional order system depending on the value of q is provided in Fig. 4.

3.4. Fractional order PID (FOPID) controller

The FOPID controller denoted by $(PI^{\alpha}D^{\beta})$ was first proposed by Podlubny in 1999 [43]. The general structure of the FOPID controller is given by

$$ G_{FOPID}(s) = \frac{U(s)}{E(s)} = k_{p} + \frac{k_{i}}{s^{\alpha}} + k_{d} s^{\beta} \tag{14} $$

where, $U(s)$ is controller output, $E(s)$ is error, k_P, k_I, and k_D are proportional, integral, and derivative gain and $0 \leqslant \alpha, \beta \leqslant 2$.

The integrator and derivative term on a semi-logarithmic plane represents a line with -20α dB [20] and $+20\beta$ dB slope. Fig. 5 represents the block diagram configuration of the FOPID controller.

Clearly, $\lambda = \mu = 1$ represents a conventional PID controller. The selection of $\alpha = 0, \beta = 1$ and $\alpha = 1, \beta = 0$ represents the integer order of the PD and PI controller respectively. All these classical controllers are the special cases of the fractional order PID controller. This same concept has been pictorially represented in Fig. 6

The controller that we have discussed represents a 1-DOF structure. When a 1-DOF PID controller is designed for a highly unstable system, it usually exhibits large overshoots because of the presence of the controller zeros at inappropriate positions in the closed-loop input-output transfer function. The controller output becomes also high as these zeros occur in a closed loop transfer function from the reference input to the controller output. These problems have been eliminated by using a 2-DOF controller. For the 2-DOF PID controller, a feed forward compensator (PD controller) and a serial compensator (PID controller) are present, as shown in Fig. 7.

3.5. FOPID controller design

For the ease of implementation in hardware and to carry out simulations in a digital computer fractional order derivatives and integrals are often realized by integer order approximations. To obtain a transfer function with a finite number of poles and zeros,

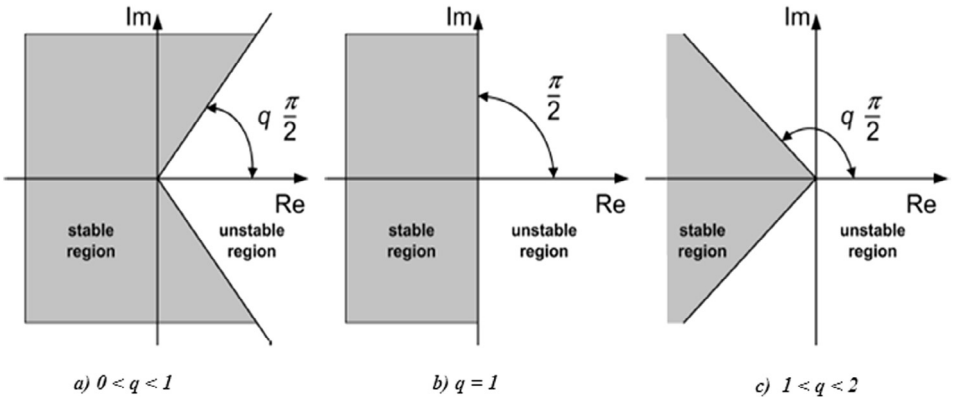

Fig. 4. Region of stability of LTI fractional order system for different value of q.

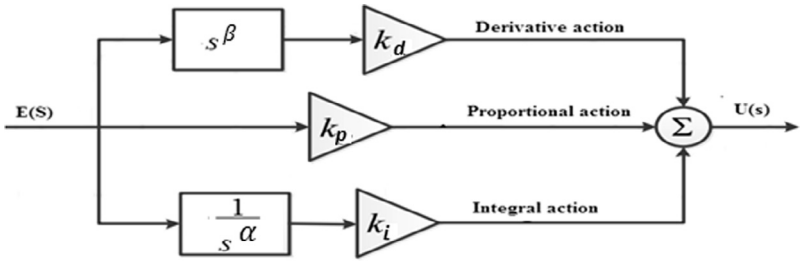

Fig. 5. Fractional Order PID controller.

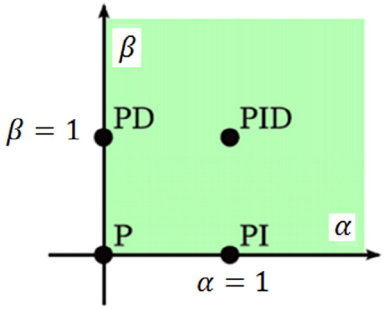

Fig. 6. General form of FOPID controller.

this paper incorporates the use of integer order approximations by Oustaloup based on the recursive distribution of poles and zeros [40,44]. The transfer function of the Oustaloup filter can be designed as

$$G_f(s) = k\prod_{r=1}^{N}\frac{s+\omega_r'}{s+\omega_r} = s^{\gamma} \tag{15}$$

$$\text{Where } \omega_r' = \omega_l\omega_u^{\frac{(2r-1-\gamma)}{N}} \tag{16}$$

$$\omega_r = \omega_l\omega_u^{\frac{(2r-1+\gamma)}{N}} \tag{17}$$

$$k = \omega_h^{\gamma} \tag{18}$$

$$\omega_u = \sqrt{\frac{\omega_h}{\omega_l}} \tag{19}$$

where, N is the order of the filter which can be either an even or odd integer, γ is the order of the derivative, k is the filter gain, ω_l, ω_h are lower and higher cut off frequencies. The above approximation holds true in the frequency range $[\omega_l, \omega_h]$. Gain K is selected to obtain a unit gain at 1 rad/s. The order of the filter (i.e. number of poles and zeros) is chosen in such a way that the desired performance is achieved. The low value of N results in simpler approximations, but increases the chance of the appearance of ripples in both gain and phase behaviours, whereas a high value of N eliminates the ripple but makes the approximation computationally expensive.

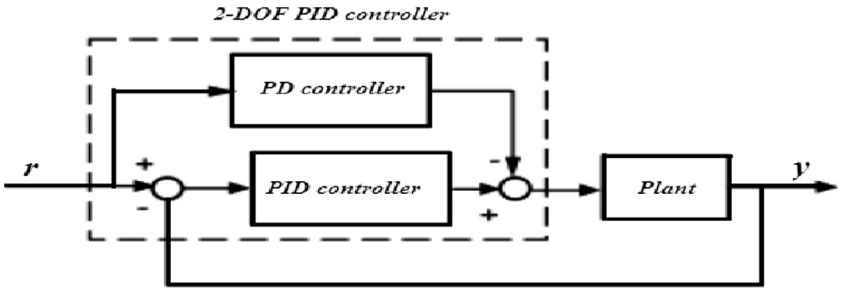

Fig. 7. 2-DOF PID controller.

The Eq. (15) can be inverted to handle the cases where $\gamma < 0$. If the order of the derivative (γ) is greater than 1, then the fractional order of 's' can be transformed as follows

$$s^{\gamma} = s^{a}s^{d}, \gamma = a + d, a \in z, d \in [0, 1] \tag{20}$$

So 'a' being an integer the only approximation that has to be performed is for s^d. Throughout the simulation, the application of the CRONE (Commande Robusted'Ordre Non Entier, meaning Non-Integer-Order Robust Control) method developed by Ousatloop is employed. The Non Integer (Ninteger) order block in Matlab has been employed to design fractional order differentiators and integrators leading to the design of the FOPID controller in Simulink and during validation of the results using the experimental set of Maglev plant.

4. Fractional order PID controller design formulation

4.1. Dominant pole calculation

This paper incorporates the linearized version of the nonlinear Maglev plant as explained in Section 2. The design specifications for this study have been taken as

Damping ratio $\zeta = 0.8$ and

Settling time $t_s = \dfrac{4}{\zeta w_n} \leqslant 2$ s

According to these specifications, dominant poles obtained by solving the characteristic equation $s^2 + 2\zeta w_n s + w_n^2 = 0$ are

$$s_{1,2} = -2 \pm 1.5i \tag{21}$$

4.2. Objective function formulation

The value of the controller parameters can be found by minimizing the objective function $f = |R| + |I|$, where R and I are the real and imaginary part of the characteristics equation after substituting the dominant pole obtained from satisfying the design specifications. Under ideal conditions, after optimization the value of the objective function will be equal to zero.

Substituting the dominant pole s_1 in the characteristic equation we get

$$1 + G_p(s_1)G_c(s_1) = 0 \tag{22}$$

For conventional and for fractional order PID controller $G_c(s_1)$ is equal to $\left(k_p + \frac{k_i}{s_1} + k_d s_1\right)$ and $\left(k_p + \frac{k_i}{s_1^{\beta}} + k_d s_1^{\beta}\right)$ respectively. Where, k_p = proportional gain, k_i = integral gain, k_d = derivative gain, α and β are the fractional power of s and lies in between 0.1 and 2.

The estimation of controller parameters has been framed as an optimization which seeks to minimize the real and imaginary component of the characteristic equation. Starting with a set of random model parameters, they are iteratively updated till a pre-defined convergence criterion is met. The objective function can be framed as

$$f = |Real(1 + G_p(s_1)G_c(s_1)| + |Imaginary(1 + G_p(s_1)G_c(s_1)| \tag{23}$$

4.3. System with 1-DOF IOPID

The closed loop representation of the Maglev system with 1-DOF IOPID controller is shown in Fig. 8

Characteristics equation of the Maglev system with 1-DOF IOPID controller for unity feedback is given by

$$1 + G_p(s)G_c(s) = 0 \tag{24}$$

$$i.e\ 1 + \left(\frac{b}{s^2 - p^2}\right)\left(k_p + \frac{k_i}{s} + k_d s\right) = 0 \tag{25}$$

$$i.e.\ 1 + \left(\frac{-3518.85}{s^2 - 2180}\right)\left(k_p + \frac{k_i}{s} + k_d s\right) = 0 \tag{26}$$

Substituting the value of s_1 in the above equation and separating real (R) and imaginary (I) parts, one obtains

$$R = 1 + 1.6154k_p - 0.5180k_i - 3.2242k_d \tag{27}$$

$$I = -0.0044k_p - 0.3863k_i + 2.4319k_d \tag{28}$$

The objective function 'f' considered for obtaining the value of k_p, k_i and k_d has the following format

$$f = |R| + |I| \tag{29}$$

4.4. System with 1-DOF FOPID

The closed loop representation of the Maglev system with 1-DOF FOPID controller is shown in Fig. 9

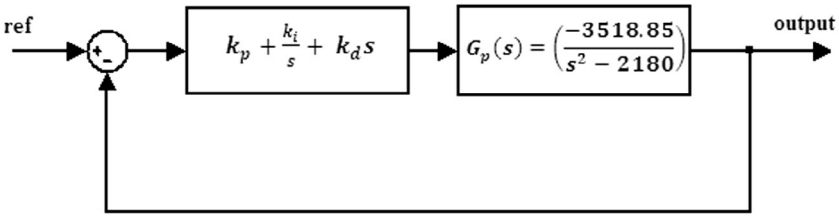

Fig. 8. 1-DOF IOPID controller with Maglev system.

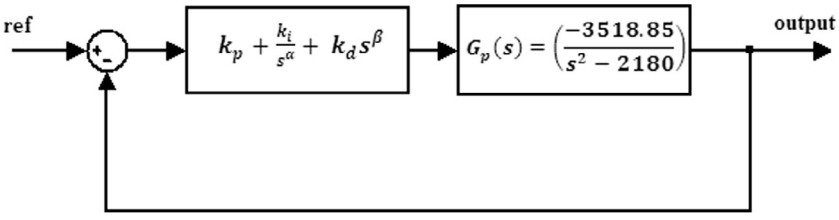

Fig. 9. 1-DOF FOPID controller with Maglev system.

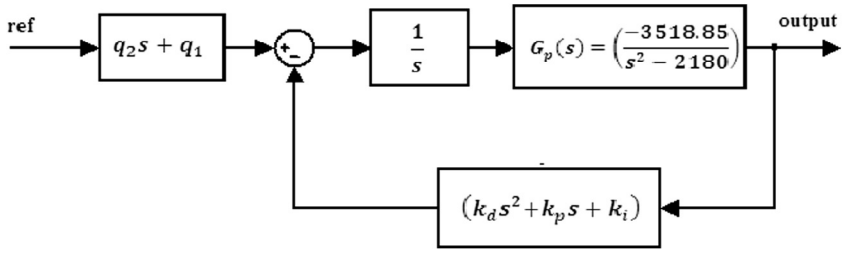

Fig. 10. 2-DOF IOPID controller with Maglev system.

Characteristics equation of the Maglev system with 1-DOF FOPID for unity feedback is given by

$$1 + G_p(s)G_c(s^{\alpha,\beta}) = 0 \tag{30}$$

$$i.e\ 1 + \left(\frac{b}{s^2 - p^2}\right)\left(k_p + \frac{k_i}{s^\alpha} + k_d s^\beta\right) = 0 \tag{31}$$

$$i.e.\ 1 + \left(\frac{-3518.85}{s^2 - 2180}\right)\left(k_p + \frac{k_i}{s^\alpha} + k_d s^\beta\right) = 0 \tag{32}$$

In the same way, substituting the value of s_1 in the above equation and separating real (R) and imaginary (I) parts, one obtains

$$R = 1 + 1.6154k_p + \left(\frac{1.6154}{2.5^\alpha} \times \cos(2.4981\alpha) - \frac{0.0044}{2.5^\alpha} \times \sin(2.4981\alpha)\right)k_i + \left(1.6154 \times 2.5^\beta \times \cos(2.4981\beta) + 0.0044 \times 2.5^\beta \times \sin(2.4981\beta)\right)k_d \tag{33}$$

$$I = -0.0044k_p + \left(\frac{-1.6154}{2.5^\alpha} \times \sin(2.4981\alpha) - \frac{0.0044}{2.5^\alpha} \times \cos(2.4981\alpha)\right)k_i + \left(1.6154 \times 2.5^\beta \times \sin(2.4981\beta) - 0.0044 \times 2.5^\beta \times \cos(2.4981\beta)\right)k_d \tag{34}$$

The objective function for finding k_p, k_i, k_d, α and β has the same format as given in Section 4.3.

4.5. System with 2-DOF IOPID

The closed loop representation of the Maglev system with 2-DOF IOPID controller is shown in Fig. 10. The idea of this kind of structure came from the general feed forward type 2-DOF dynamic controller discussed in [35]. The presence of additional gain parameters q_1 ($q_1 = k_i$) and q_2 (tuned to obtain the desired speed of response) helps to add a zero at the desired location to achieve a superior response as compared to its 1-DOF counterpart.

Characteristics equation of the Maglev system with 2-DOF IOPID controller is given by

$$1 + \left(\frac{b}{s^2 - p^2}\right)\left(\frac{k_d s^2 + k_p s + k_i}{s}\right) = 0 \tag{35}$$

Again, in the same way, substituting the value of s_1 in the above equation and separating real (R) and imaginary (I) parts, one obtains

$$R = 0.6203 + k_p - 0.5k_i - 0.8750k_d \tag{36}$$

$$I = -0.4626 - 0.75k_p + 3k_d \tag{37}$$

The structure of the objective function for finding the unknown parameters remains same as described in Section 4.3.

Table 2
Range of Parameters for 1-DOF IOPID.

PID parameters	Initial guess	Lower value	Upper value
k_p	−2.65	−3	−2
k_i	−2.65	−3	−2
k_d	−0.5	−0.7	−0.2

Table 3
Final values of Parameters for 1-DOF IOPID.

k_p	k_i	k_d
−2.3973	−2.7749	−0.4451

Table 4
Range of Parameters for 1-DOF FOPID.

PID parameters	Initial guess	Lower value	Upper value
k_p	−4	−4.5	−3.5
k_i	−4.5	−5	−4
k_d	−0.4	−0.2	0
α	0.7	0.1	0.875
β	0.95	0.1	1

Table 5
Final values of Parameters for 1-DOF FOPID.

k_p	k_i	k_d	α	β
−3.5	−4	−0.2	0.875	1

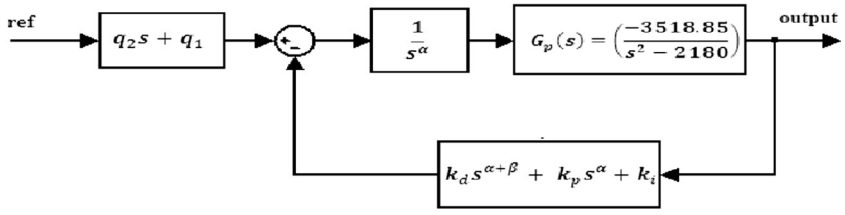

Fig. 11. 2-DOF FOPID controller with Maglev system.

Table 6
Range of Parameters for 2-DOF IOPID.

PID parameters	Initial guess	Lower value	Upper value
k_p	−2.6	−3.5	−2.5
k_i	−2.4	−2.75	−1.75
k_d	−0.05	−0.15	0

Table 7
Final values of Parameters for 2-DOF IOPID.

k_p	k_i	k_d
−2.5	−2.75	−0.15

Table 8
Range of Parameters for 2-DOF FOPID.

PID parameters	Initial guess	Lower value	Upper value
k_p	−2	−2.5	−1.5
k_i	−3	−3.7	−2.7
k_d	−0.05	−0.15	0
α	0.9	0.1	0.875
β	0.6	0.1	0.8

Table 9
Final values of Parameters for 2-DOF FOPID.

k_p	k_i	k_d	α	β
−1.5	−2.7	−0.15	0.875	0.8

4.6. System with 2-DOF FOPID

The closed loop representation of the Maglev system with 2-DOF FOPID controller is shown in Fig. 11.

The Characteristics equation of the Maglev system with 2-DOF FOPID for unity feedback is given by

$$1 + \left(\frac{b}{s^2 - p^2}\right)\left(\frac{k_d s^{\alpha+\beta} + k_p s^{\alpha} + k_i}{s^{\alpha}}\right) = 0 \tag{38}$$

In the same way, substituting the value of s_1 in the above equation and separating real (R) and imaginary (I) parts, one obtains

$$\begin{aligned} R = {} & -0.6190 \times 2.5^{\alpha} \times \cos(2.4981\alpha) + 0.0017 \times 2.5^{\alpha} \\ & \times \sin(2.4981\alpha) - 2.5^{\alpha} \times cos(2.4981\alpha) \times k_p - k_i \\ & - 2.5^{\alpha+\beta} \times cos(2.4981 \times (\alpha+\beta)) \times k_d \end{aligned} \tag{39}$$

$$\begin{aligned} I = {} & -0.0017 \times 2.5^{\alpha} \times \cos(2.4981\alpha) - 0.6190 \times 2.5^{\alpha} \\ & \times \sin(2.4981\alpha) - 2.5^{\alpha} \times sin(2.4981\alpha) \times k_p \\ & - 2.5^{\alpha+\beta} \times sin(2.4981 \times (\alpha+\beta)) \times k_d \end{aligned} \tag{40}$$

The objective function for finding the value of k_p, k_i, k_d, α and β has the same format as described in Section 4.3

4.7. Parameter optimization for IOPID and FOPID systems

The objective function has been optimized using the nonlinear interior point optimization function in MATLAB subjected to

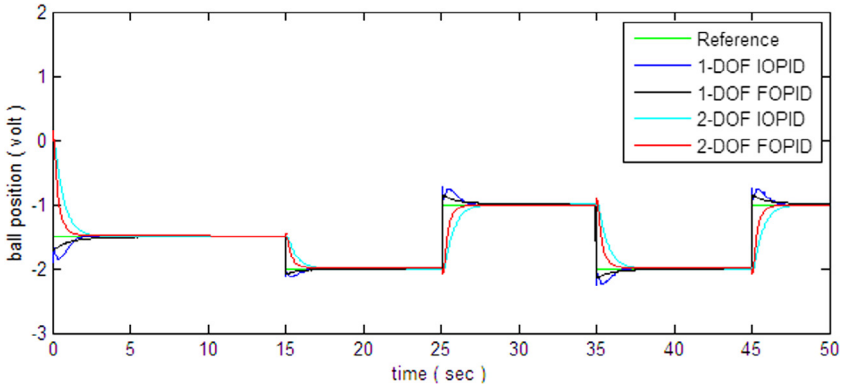

Fig. 12. Simulink response of Maglev system with 1-DOF and 2-DOF IOPID and FOPID controller.

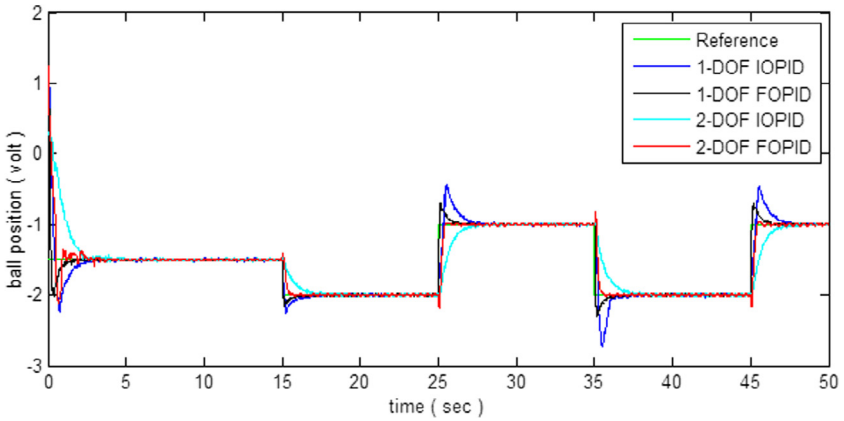

Fig. 13. Real-time response of Maglev system with 1-DOF and 2-DOF IOPID and FOPID controller.

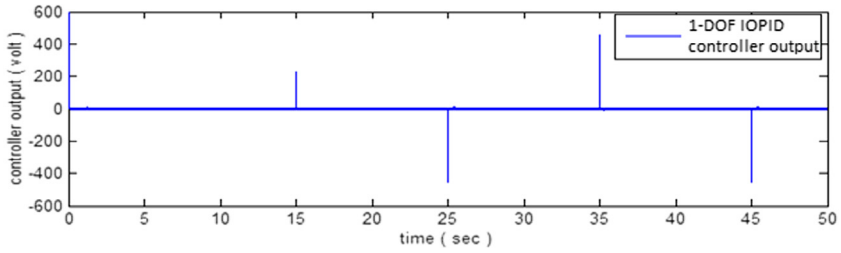

Fig. 14. 1-DOF IOPID controller output (real time).

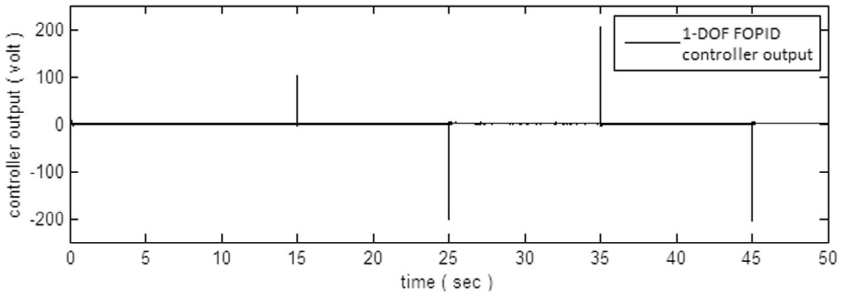

Fig. 15. 1-DOF FOPID controller output (real time).

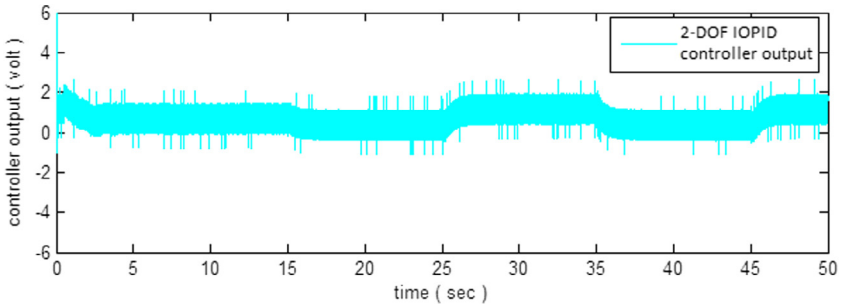

Fig. 16. 2-DOF IOPID controller output (real time).

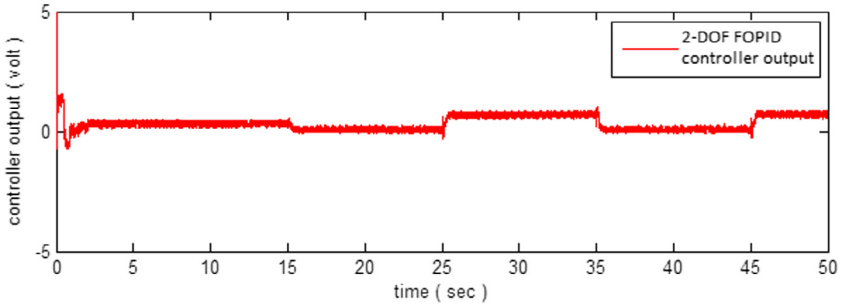

Fig. 17. 2-DOF FOPID controller output (real time).

Table 10
Time domain specifications of the Maglev system with different controllers.

Controller	Maximum overshoot (%)	Peak time (sec)	Rise time (sec)	Delay time (sec)	Settling time (sec)
1-DOF IOPID	57.03	0.56	0.3	0.3	2.83
1-DOF FOPID	30.66	0.13	0.05	0.15	1.54
2-DOF IOPID	1.86	3.6	1.21	0.66	3.06
2-DOF FOPID	2.4	0.63	0.3	0.35	0.85

various constraints, and bounded within a certain range. The algorithm for the nonlinear interior point optimization method is given below.

$$Minimize\ f(x)$$

$$subjectto\ h_i(x) = 0, \quad i = 1, 2, \ldots\ldots\ldots, p$$

$$g_j(x) \le 0, \quad j = 1, 2, \ldots\ldots\ldots, m$$

where $f(x)$ represents the nonlinear function, $h_i(x)$ with i ranging from 1 to p represents p equality constraints and

$$g_j(x)$$

with j ranging from1 to m represents m inequality constraints. The interior penalty function can be formulated as

$$P(x, \gamma_k) = f(x) + \gamma_k \sum_{j=1}^{m} - \frac{1}{g_j(x)} f$$

Where $\gamma_k > 0$ represents penalty coefficients and $P(x, \gamma_k)$ represents the penalty function.

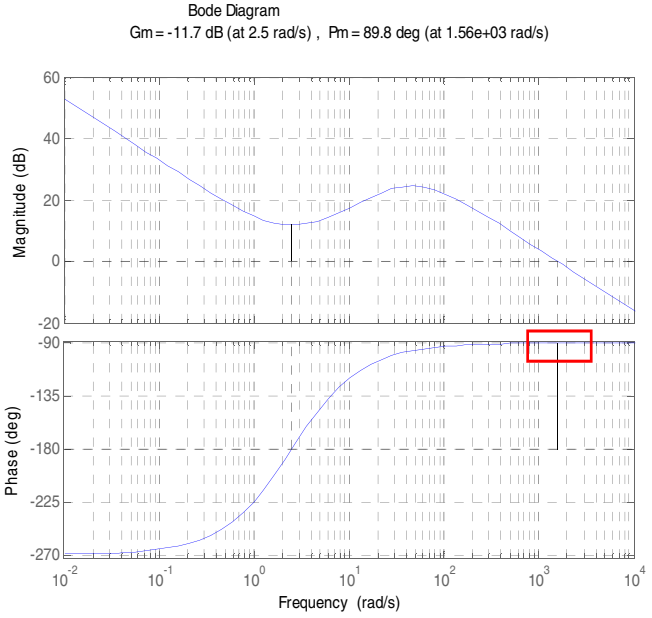

Fig. 18. Bode Plot of Maglev system with 1-DOF IOPID showing flatter phase curve (red box) around gain cross over frequency.

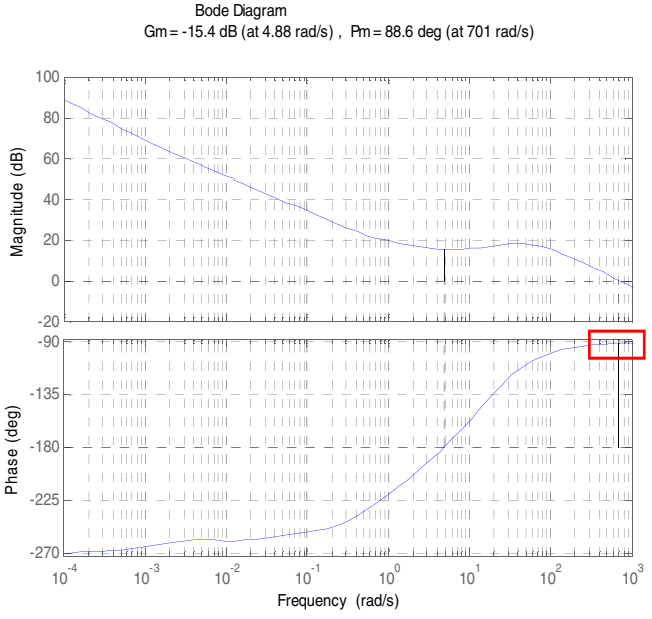

Fig. 19. Bode Plot of Maglev system with 1-DOF FOPID showing flatter phase curve (red box) around gain cross over frequency. (For interpretation of the references to colour in this figure legend, the reader is referred to the web version of this article.)

Algorithmic Steps:

Step 1: Select a feasible solution $x^{(0)}$ (Interior point) that satisfies all constraints, $g_j(x) \le 0, j = 1, 2, \ldots\ldots\ldots, m$ and select $\gamma_k > 0, k = 1$.

Step 2: Take $x^{(k-1)}$ as a starting point and use any one of the unconstrained minimization numerical methods (Newton Raphson, Steepest Descent or Conjugate Gradient method) to find the optimum of the barrier function or Interior penalty function, denoted by x^k.

Step 3: Check if the solution x^k is the optimum solution of the original problem

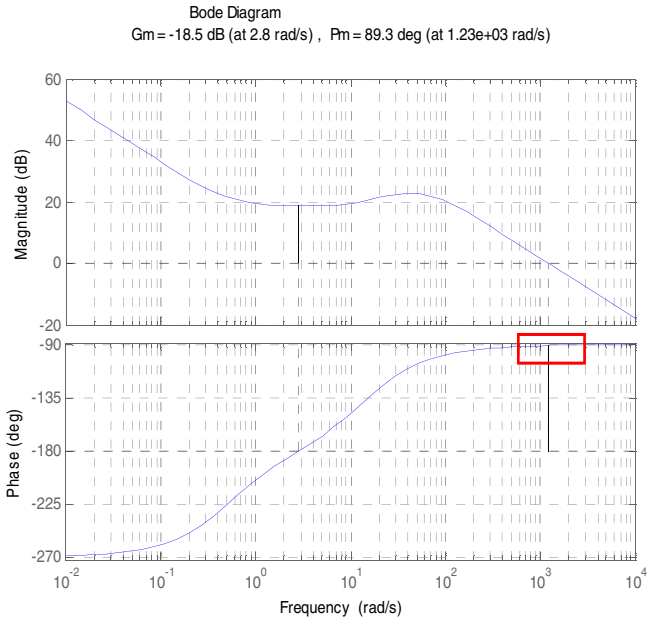

Fig. 20. Bode Plot of Maglev system with 2-DOF IOPID showing flatter phase curve (red box) around gain cross over frequency. (For interpretation of the references to colour in this figure legend, the reader is referred to the web version of this article.)

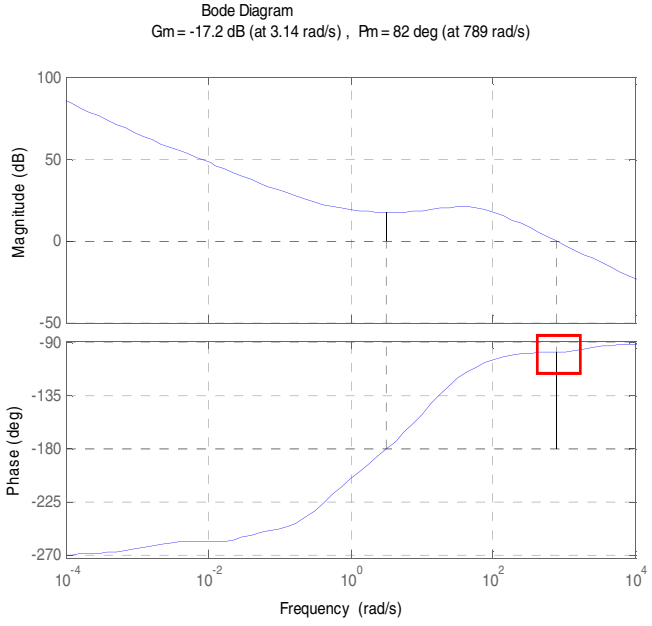

Fig. 21. Bode Plot of Maglev system with 2-DOF FOPID showing flatter phase curve (red box) around gain cross over frequency. (For interpretation of the references to colour in this figure legend, the reader is referred to the web version of this article.)

$$\left|\frac{f(x^{(k)}) - f(x^{(k-1)})}{f(x^{(k)})}\right| \leqslant \in_1 \text{or}$$

$$\gamma_k F(x^{(k)}) \leqslant \in_2$$

where $\gamma_k > 0, \in_1, \in_2 > 0, F(x^{(k)}) = \sum_{j=1}^{m} -\frac{1}{g_j(x)}$, otherwise go to the next step

Step 4: Set $\gamma_{k+1} = c\gamma_k$, where $c < 1$. Set $k = k + 1$ and go to Step 2

The initial guess, ranges of the parameters and the values obtained after optimization have been provided in Tables 2–9. The Routh Hurwitz criteria have been applied to the characteristic equation in (26, 32, 35, 38) to obtain the ranges of k_p, k_i, and k_d. The lower and upper ranges of the parameters have been decided after a number of trial runs. Applying Routh Hurwitz criteria, it can be deduced that k_p, k_i, and k_d has to be negative in the case of IOPID and FOPID controller configurations for making the closed loop system stable. The sample MATLAB script for optimizing the objective function has been provided in Appendix 1.

5. Simulink and real time responses

The input signal considered for this study is a square wave with a mean of −1.5 V. The FOMCON toolbox has been used for the analysis of the region of stability of the closed loop system with fractional order controllers.

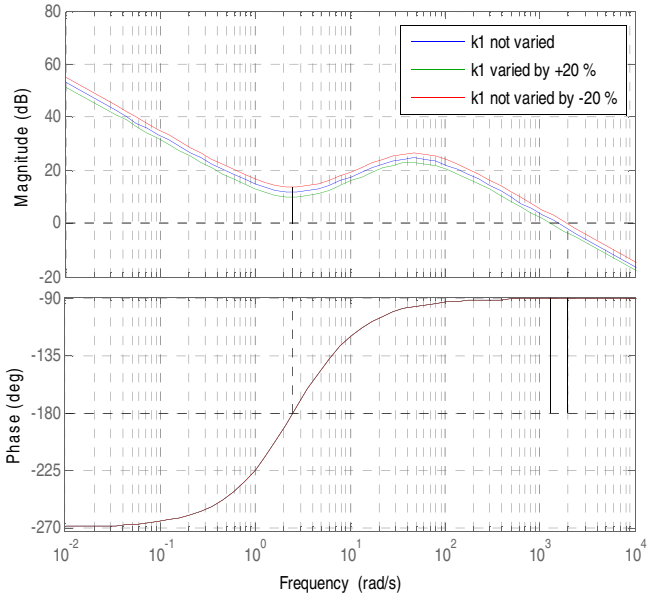

Fig. 22. Bode Plot of Maglev system with 1-DOF IOPID controller by varying k_1 from −20% to +20%.

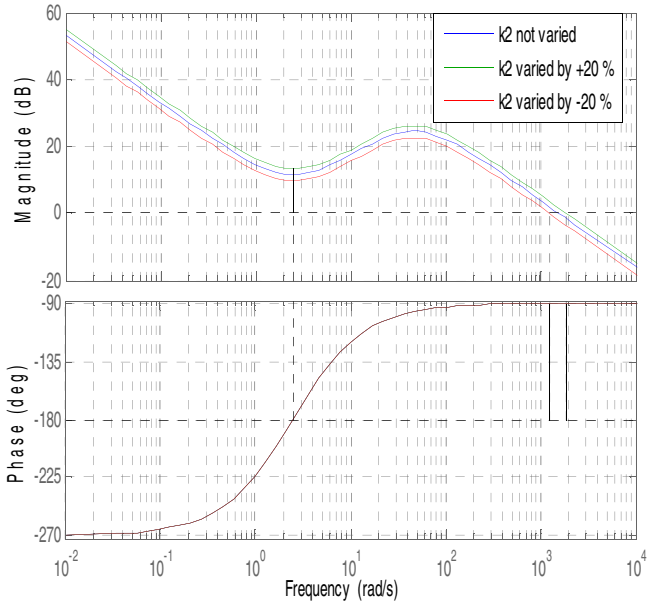

Fig. 23. Bode Plot of Maglev system with 1-DOF IOPID controller by varying k_2 from −20% to +20%.

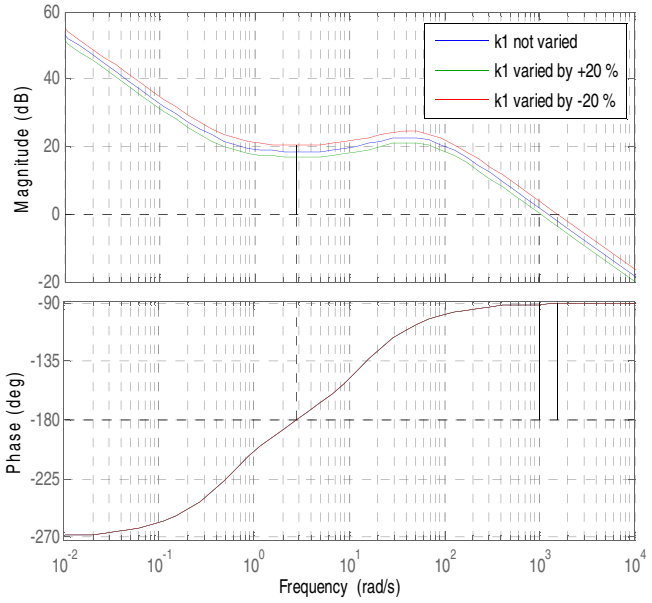

Fig. 24. Bode Plot of Maglev system with 2-DOF IOPID controller by varying k_1 from −20% to +20%.

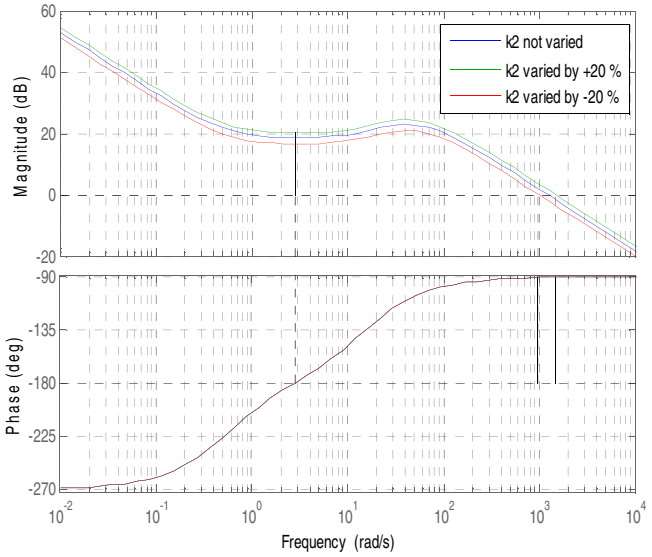

Fig. 25. Bode Plot of Maglev system with 2-DOF IOPID controller by by varying k_2 from −20% to +20%.

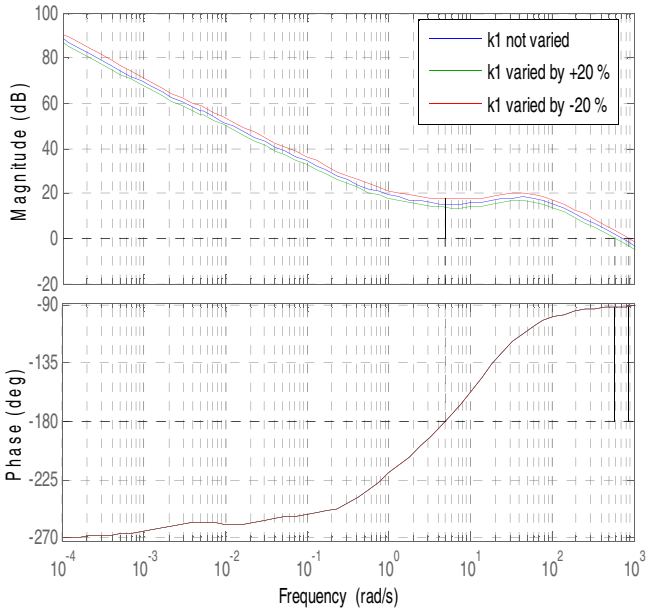

Fig. 26. Bode Plot of Maglev system with 1-DOF FOPID controller by varying k_1 from −20% to +20%.

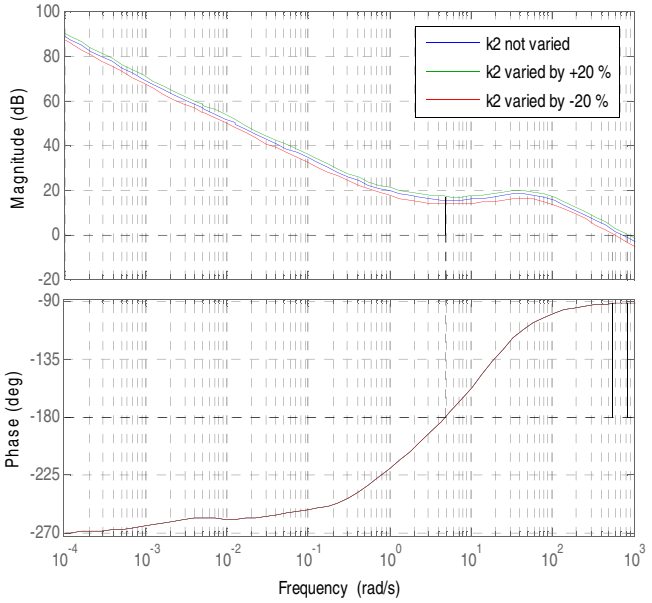

Fig. 27. Bode Plot of Maglev system with 1-DOF FOPID controller by varying k_2 from −20% to +20%.

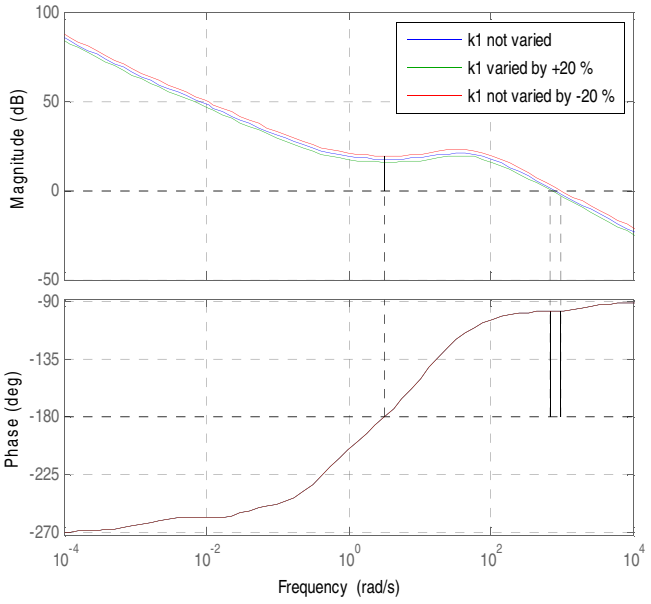

Fig. 28. Bode Plot of Maglev system with 2-DOF FOPID controller by varying k_1 from −20% to +20%.

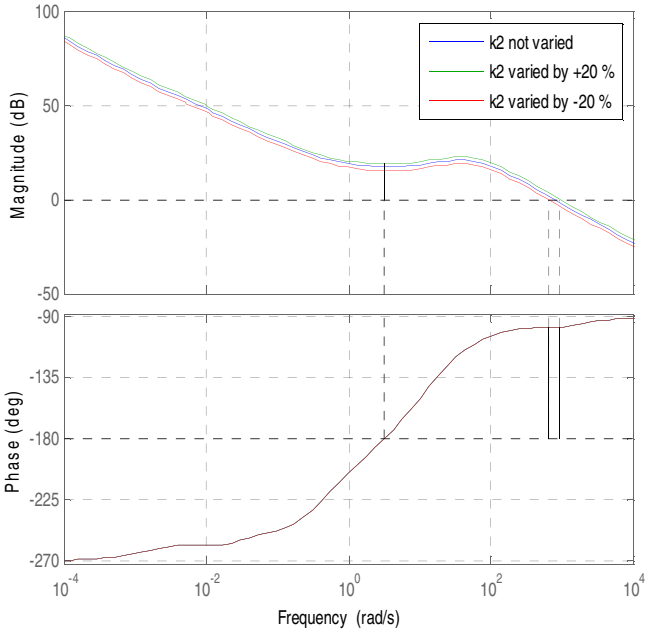

Fig. 29. Bode Plot of Maglev system with 2-DOF FOPID controller by by varying k_2 from −20% to +20%.

The closed loop response of the 1-DOF and 2-DOF IOPID and FOPID controllers along with the controller output during simulation and in real time are shown in Figs. 12–17. It is clear from the figures that, as the controller structure migrate from 1-DOF to 2-DOF and IO to FO, the response of the system and the controller output improve. The best response that we have witnessed is in the case of the 2-DOF FOPID controller.

5.1. Performance comparison between different controllers

The real-time response of the Maglev system with 1-DOF and 2-DOF IOPID and FOPID controllers has been compared and summarized in Table 10 which reflects the superiority of the 2-DOF FOPID controller over other genres of controllers in generating better transient response. The maximum overshoot in the case of the 2-DOF IOPID is better than that of the 2-DOF FOPID, but the other transient parameters (Peak time, Rise time, Delay time and Settling time) are far better and optimal in case of a 2-DOF FOPID.

6. Robustness analysis

The robustness of a control system accounts for both environmental changes and model uncertainties in real world conditions.

Table 11
Robustness analysis of the Maglev system with different controllers.

Controller	Gain Crossover Frequency (w_g) in rad/s	Gain Margin (db)	Phase Margin (degrees)	Slope of the phase angle around w_g (iso-damping condition)	Sensitivity	Complementary Sensitivity
1-DOF IOPID	1564	−11.7	89.8	$4.57 * 10^{-7}$	1	1.3498
1-DOF FOPID	700.80	−15.4	88.6	$4.56 * 10^{-6}$	1	1.1951
2-DOF IOPID	1229	−18.5	89.3	$1.73 * 10^{-5}$	1	1.1344
2-DOF FOPID	788.73	−17.2	82	$4.87 * 10^{-5}$	1	1.1604

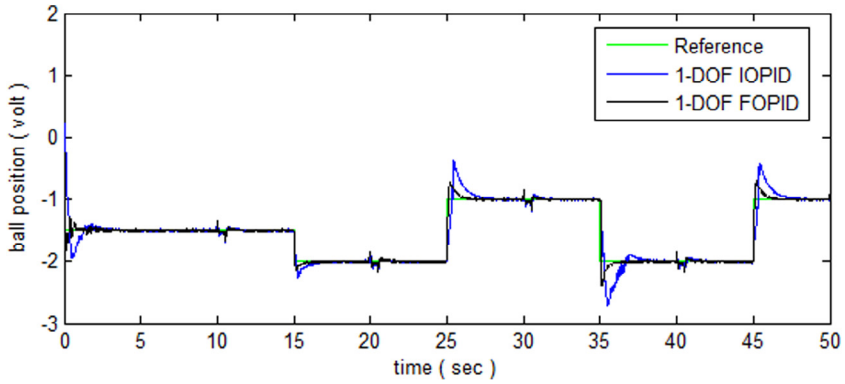

Fig. 30. Response of Maglev system with 1-DOF IOPID and FOPID controller to periodic output disturbance (real time).

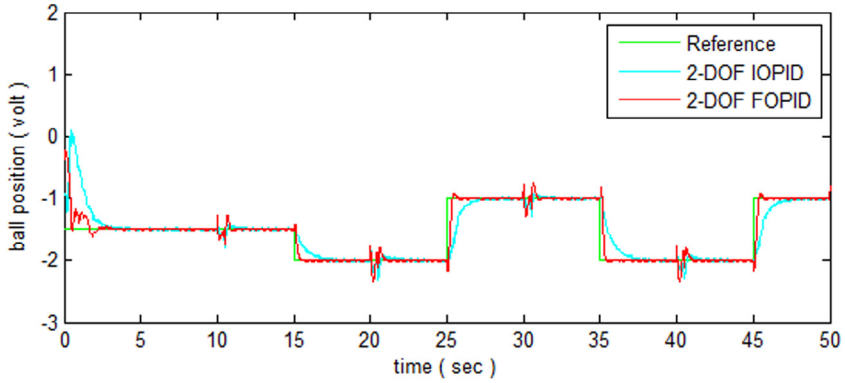

Fig. 31. Response of Maglev system with 2-DOF IOPID and FOPID controller to periodic output disturbance (real time).

Two properties determine this concept of system robustness: sensitivity and disturbance rejection. Here, the robustness of both the FOPID and IOPID systems in 1-DOF and 2-DOF configurations is studied through MATLAB simulations and real time experiments. The robustness has been evaluated in terms of gain crossover frequency, phase margin, gain margin and the isodamping property, which are respectively represented as with the obtained $k_p, k_i, and k_d$ for different controller configurations. The robustness indices are given as:

$$|G_c(jw_{gc}).G(jw_{gc})| = 1 \tag{41}$$

$$Arg(G_c(jw_{gc}).G(jw_{gc})) = -\pi + \phi_{pm} \tag{42}$$

$$\frac{d(Arg(G_c(jw_{gc}).G(jw_{gc})))}{dw} = 0 \text{ (Isodamping property)} \tag{43}$$

where, $|G_c(jw_{gc})| = k_p + \frac{k_i}{jw_{gc}} + k_d jw_{gc}$, $G(jw_{gc}) = Planttransferfunction$, $w_{gc} = Gaincrossoverfrequency$, $\phi_{pm} = Desiredphasemargin$

The magnitude and phase plot of the open loop transfer function for different controller configurations with the plant are shown in Figs. 18–21.

It can be verified from the Figs. 18–21 that the open loop phase plot in the case of IOPID and FOPID controller has a flatter phase curve denoted by a red box around the gain cross over frequency satisfying the iso-damping property. Further from the Figs. 22–29, it can be observed that as the coil current constant (k_1) and the sensor gain constant (k_2) varies between −20% and +20%, the open loop phase plot in the case of IOPID and FOPID controller exhibit a flatter phase curve around the gain crossover frequency ensuring good loop robustness to model uncertainties. Table 11 shows the gain margin, phase margin, gain cross-over frequency, and slope of the phase curve around the gain cross-over frequency (iso-damping condition) for 1-DOF and 2-DOF IOPID and FOPID controller with the Maglev plant. The Nyquist plot in Appendix 1 can also demonstrate the fact that even if the Gain Margin of the open loop unstable magnetic levitation system with different controller configurations is negative, the overall closed

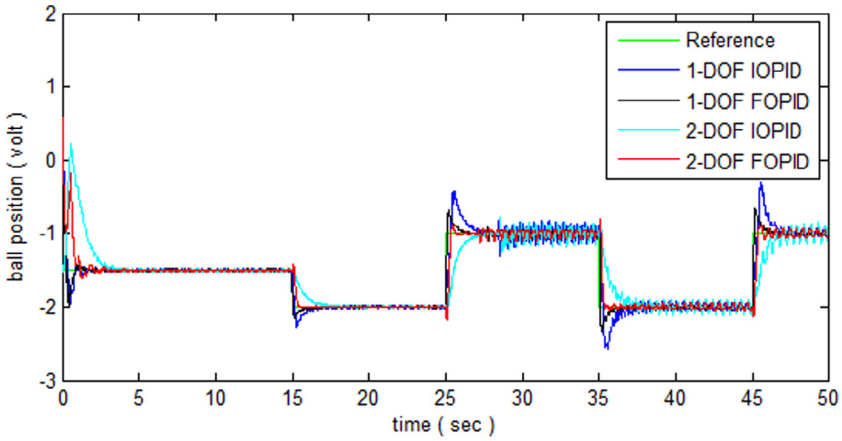

Fig. 32. Response of Maglev system with 1-DOF and 2-DOF IOPID as well as FOPID controller to external physical (hand-held) disturbance.

loop system is stable. The robustness of the system is verified during real time experiments by subjecting both the IOPID and FOPID controller based 1-DOF and 2-DOF MAGLEV system to output disturbance addition as well as hand-held disturbance.

For experimental data analysis, a pulse magnitude of 0.225V (i.e. 15% of the input voltage) at intervals of 10 s each was applied and the responses of all the above-mentioned systems are shown in Figs. 30 and 31.

Also, the behaviour of the compensated systems, when the steel ball was physically disturbed by hand was recorded, and the responses are shown in Fig. 32. In the hand-held disturbance case the external disturbance was applied between 25 s and 30 s.

It is quite clear from the above results that in the case of both the 1-DOF and the 2-DOF systems, the fractional order controller is showing a more robust behaviour compared to the integer order controller in rejecting periodic disturbances and external physical disturbances. The proposed 2-DOF FOPID controller exhibits superior periodic disturbance rejection compared to the 1-DOF IOPID, 1-DOF FOPID and 2-DOF IOPID. This result indicates the superiority of the FOPID system over the IOPID system.

7. Conclusion

In this paper, a simple and elegant method for the design of a FOPID controller based on the dominant pole placement method is proposed. The IOPID and FOPID parameters are obtained from the dominant pole placement method by optimizing the objective function, using the nonlinear interior point optimization technique. Robustness verification is also performed to ensure the ability of the controller to withstand the model uncertainties in terms of disturbance rejection. The model responses obtained from the simulation and experimental set-up suggest the superiority of the FOPID controller over the IOPID controller to track a reference trajectory. As an extension of this research work, the design of a Fractional Order sliding mode controller for a nonlinear magnetic levitation plant can also be studied, and the response obtained from simulation can be verified with the experimental set-up. The methodology employed for this model set- up can be extended to other nonlinear models, to study their closed loop behaviour under nonlinear conditions and model uncertainties.

Declaration of Conflicting Interests

'The authors declare that there is no conflict of interest'.

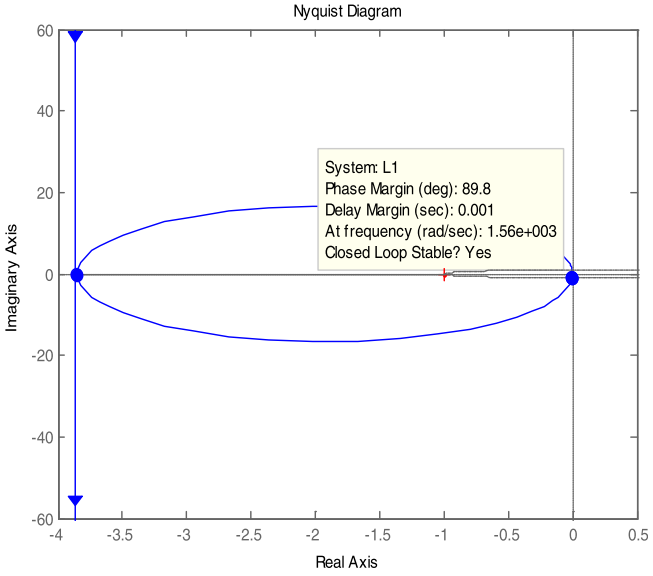

Fig. A1. Nyquist Plot of Maglev system with 1-DOF IOPID controller.

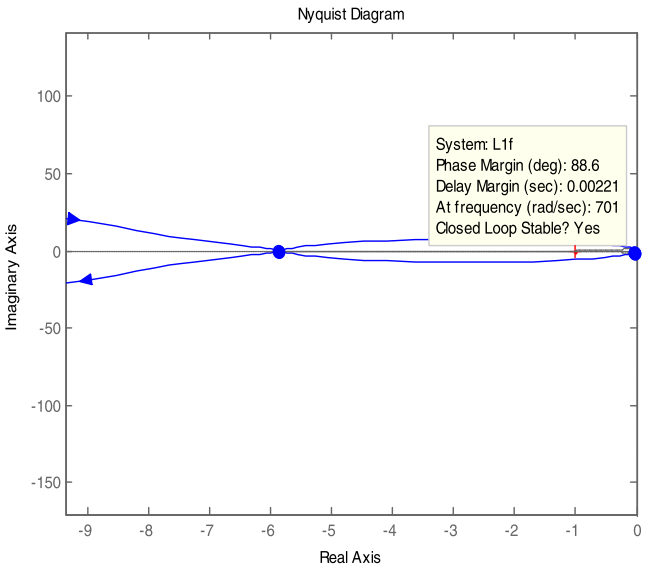

Fig. A2. Nyquist Plot of Maglev system with 1-DOF FOPID controller.

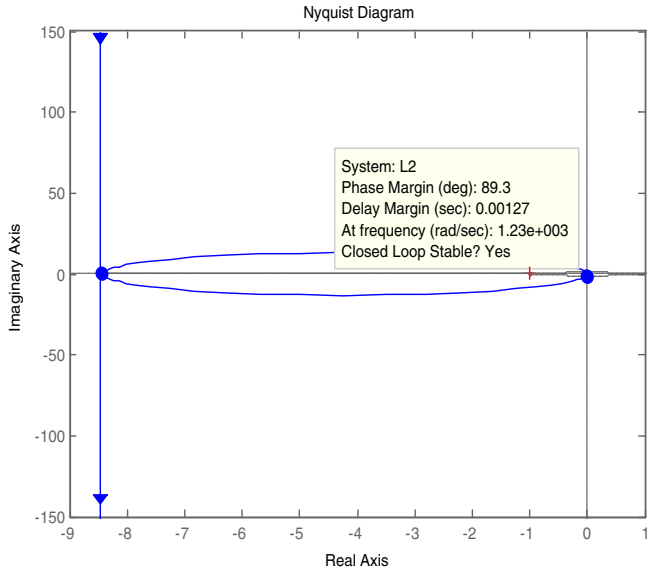

Fig. A3. Nyquist Plot of Maglev system with 2-DOF IOPID controller.

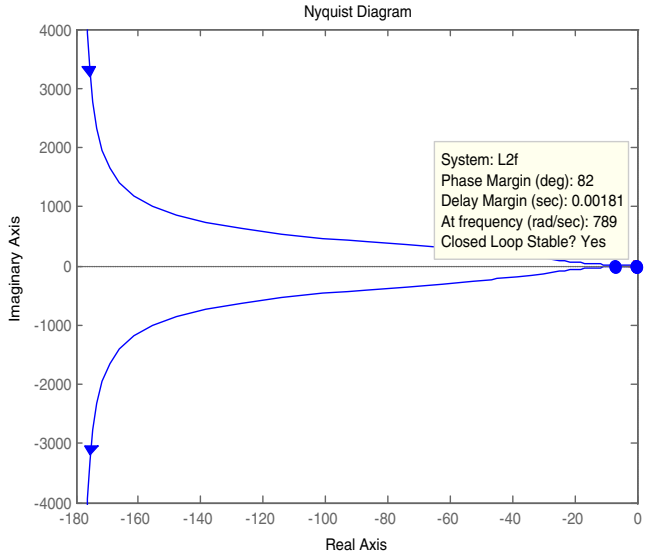

Fig. A4. Nyquist Plot of Maglev system with 2-DOF FOPID controller.

Acknowledgements

The authors would like to acknowledge the Department of Electrical and Electronics Engineering of Birla Institute of Technology (BIT), Mesra in Ranchi, India for providing adequate facilities in the Control Laboratoryto carry out the experimentation work with the Magnetic Levitation Plant from Feedback Instruments. This research received no specific grant from any funding agency in the public, commercial, or not-for-profit sectors.

Appendix 1

The MATLAB script for finding the 1-DOF and 2-DOF IOPID and FOPID controller parameter values by optimizing the objective function is given below. 'Fmincon' (nonlinear interior point optimization technique) is the Matlab command used in this research work for the function minimization.

```
% MATLAB script for finding 1-DOF IOPID controller parameter values

% Objective function denoted by the variable fun
fun=@(x)(abs(1+1.6154*x(1)-0.5180*x(2)-3.2242*x(3))...
    +abs(-0.0044*x(1)-0.3863*x(2)+2.4319*x(3)))
lb = [-3,-3,-0.7];
ub = [-2,-2,-0.2]
A = [];
b = [];
Aeq = [];
beq = [];
x0 = [-2.65,-2.65,-0.5];
x = fmincon(fun,x0,A,b,Aeq,beq,lb,ub)

% MATLAB script for finding 1-DOF FOPID controller parameter values

% Objective function denoted by the variable fun
fun=@(x)(abs(1+ 1.6154*x(1)+((1.6154*x(2))...
    /(2.5^x(4)))*cos(2.4981*x(4))+((1.6154*...
    x(3))*(2.5^x(5)))*cos(2.4981*x(5))+...
    ((-0.0044*x(2))/(2.5^x(4)))*sin(2.4981*x(4))...
    -((-0.0044*x(3))*(2.5^x(5)))*sin(2.4981*x(5)))...
    +abs(-0.0044*x(1)-((1.6154*x(2))/(2.5^x(4)))*...
    sin(2.4981*x(4))+((1.6154*x(3))*(2.5^x(5)))*...
    sin(2.4981*x(5))+((-0.0044*x(2))/(2.5^x(4)))*...
    cos(2.4981*x(4))+((-0.0044*x(3))*(2.5^x(5)))*...
    cos(2.4981*x(5))))

lb = [-4.5,-5,-0.2,0.1,0.1];
ub = [-3.5,-4,0,0.875,1]
A = [];
b = [];
Aeq = [];
beq = [];
x0 = [-4,-4.5,-0.4,0.7,0.95];
x = fmincon(fun,x0,A,b,Aeq,beq,lb,ub)


% MATLAB script for finding 2-DOF IOPID controller parameter values

% Objective function denoted by the variable fun
fun=@(x) (1/21113.1)*(abs((4365.5+7037.7*x(1)-3518.85*x(2)-
6157.9875*x(3)))+abs((-3255.375-5278.275*x(1)+21113.1*x(3))))

lb = [-3.5,-2.75,-0.15];
ub = [-2.5,-1.75,0]
A = [];
b = [];
Aeq = [];
beq = [];
x0 = [-2.6,-2.4,-0.05];
x = fmincon(fun,x0,A,b,Aeq,beq,lb,ub)

% MATLAB script for finding 2-DOF FOPID controller parameter values

% Objective function denoted by the variable fun
fun=@(x) (1/3518.85)*abs((-2178.25*(2.5^x(4))...
*cos(2.498*x(4))+6*(2.5^x(4))*sin(2.498*x(4)))...
-3518.85*(2.5^(x(4)+x(5)))*cos(2.498*(x(4)+x(5)))...
*x(3)-3518.85*(2.5^x(4))*cos(2.498*x(4))*x(1)-3518.85...
*x(2)))+abs((-6*(2.5^x(4))*cos(2.498*x(4))-2178.25*...
(2.5^x(4))*sin(2.498*x(4))-3518.85*(2.5^(x(4)+x(5)))*...
sin(2.498*(x(4)+x(5)))*x(3)-3518.85*(2.5^x(4))*...
sin(2.498*x(4))*x(1)))

lb = [-2.5,-3.7,-0.15,0.1,0.1];
ub = [-1.5,-2.7,0,0.875,0.8]
A = [];
b = [];
Aeq = [];
beq = [];
x0 = [-2,-3,-0.05,0.9,0.6];
x = fmincon(fun,x0,A,b,Aeq,beq,lb,ub)
```

References

[1] Podlubny I, Dorcak L, Kostial I. On Fractional Derivatives, Fractional-Order Dynamic Systems and PIλDμ controllers. In: Proceedings of the 36th Conference on Decision & Control, San Diego, California, USA, December; 1997.
[2] Monje CA et al. A Fractional-order systems and controls: fundamentals and applications. Springer; 2010.
[3] Sabatier J et al. Fractional order differentiation and robust control design: crone, H-infinity and motion control. Springer; 2015.
[4] Hamamci SE. An Algorithm for Stabilization of Fractional-Order Time Delay Systems Using Fractional-Order PID Controllers. IEEE Trans Autom Control 2007;52(10):1964–9.
[5] Chengbin M, Hori Y. The application of fractional order PID controller for robust two-inertia speed control. In: Proceedings of the 4th International Power Electronics and Motion Control Conference, Xi'an; 2004.
[6] Podlubny I, Dorcak L, Kostial I. On Fractional Derivatives, Fractional-Order Dynamic Systems and controllers. In: Proceedings of the 36th Conference on Decision & Control, San Diego, California, USA; 1997.
[7] Podlubny I. Fractional-order systems and controllers. IEEE Trans Autom Control 1999;44(1):208–14.

[8] Boudjehem B, Boudjehem D. Fractional order controller design for desired response. Proc Inst Mech Eng, Part 1: J Syst Control Eng 2013;227(2):243–51.
[9] Beschi M, Padula F, Visioli A. The generalised isodamping approach for robust fractional PID controllers design. Int J Control 2015. http://dx.doi.org/10.1080/00207179.2015.1099076.
[10] Kheirizad I, Khandani K, Jalali AA. Stabilisability analysis of high-order unstable processes by fractional-order controllers. Int J Control 2013;86(2):244–52. http://dx.doi.org/10.1080/00207179.2012.723138.
[11] Kheirizad I, Khandani K, Jalali AA. Stabilization of fractional-order unstable delay systems by fractional-order controllers. J Syst Control Eng 2012;226(9):1166–73.
[12] Rahimian MA, Tavazoei MS. Stabilizing fractional-order PI and PD controllers: an integer-order implemented system approach. Proc Inst Mech Eng Part 1: J Syst Control Eng 2010;224:893–903.
[13] Saggaf UA, Mehedi I, Bettayeb M, Mansouri R. Fractional-order controller design for a heat flow process. Proc Inst Mech Eng Part 1: J Syst Control Eng 2016;230(7):680–91.
[14] Shi X, Huang J, Li H. Extended state observer-based fractional order proportional-derivative controller for precision trajectory tracking control of a novel linear motor. Proc Inst Mech Eng Part 1: J Syst Control Eng 2016;230(2):95–103.
[15] Muresan CI et al. Tuning algorithms for fractional order internal model controllers for time delay processes. Int J Control 2016;86(3):579–93. http://dx.doi.org/10.1080/00207179.2015.1086027.
[16] Vinagre BM, Podlubny I, Dorcak L, Feliu V. On fractional PID controllers: a frequency domain approach, Proceedings of IFAC Workshop on Digital Control-PID'00, Terrassa, Spain; 2000.
[17] Zhao C, Xue CD, Chen YQ. A fractional order PID tuning algorithm for a class of fractional order plants. In: Proceedings of the IEEE International Conference on Mechatronics & Automation, Niagara Falls, Canada; 2005.
[18] Monje CA et al. Proposals for fractional PID tuning, Proceedings of The First IFAC Symposium on Fractional Differentiation and its Applications (FDA04); 2004.
[19] Valerio D, Costa J. Tuning of fractional PID controllers with Ziegler-Nichols-type rules. Signal Processing 2006;86:2771–84.
[20] Faieghi MR, Nemati A. Applications of MATLAB in science and engineering. Iran: INTECH; 2011.
[21] Li M, Diao F. Fractional-order QFT Controllers for unstable plants based on Automatic Loop Shaping. In: Proceedings of the 10th World Congress on Intelligent Control and Automation, Beijing, China; 2012.
[22] Ozbaya H, Bonnetb C, Fioravanti AR. PID controller design for fractional-order systems with time delays. Syst Control Letts 2012;61:18–23.
[23] Lin C, Wang Q, Lee TH. An improvement on multivariable PID controller design via iterative LMI approach. Automatica 2004;40(3):519–25.
[24] Ozbay H, Gundes AN. Resilient PI and PD controller designs for a class of unstable plants with I/O delays. Appl Comput Math 2007;6(1):18–26.
[25] Hamidian H, Jalali AA. Calculation of PID controller parameters for unstable first order time delay systems. Int J Sci Eng Res 2011;2(3):1–6.
[26] Zamani M, Ghartemani MK, Sadati N, Parniani M. Design of a fractional order PID controller for an AVR using particle swarm optimization. Control Eng Practice 2009;17(12). pp. 17, pp. 1380-1387.
[27] Biswas A, Das S, Abraham A, Dasgupta S. Design of fractional-order P $I^{\lambda}D^{\mu}$ controllers with an improved differential evolution. Eng Appl Artif Intell 2009;22:343–50.
[28] Ranjan V, Jadhav S, Patil MD. Design of integer and fractional order PID controller using dominant pole placement method. In: International Journal of Computer Applications International Conference and Workshop on Emerging Trends in Technology; 2014.
[29] Zhe Yan et al. Tuning and application of fractional order PID controllers. In: Proceedings of 2013 2nd International Conference on Measurement, Information and Control, Harbin; 2013. pp. 955–958.
[30] Edet E, Katebi R. Design and tuning of fractional-order PID controllers for time-delayed processes. 2016 UKACC 11th International Conference on Control (CONTROL), Belfast; 2016. pp. 1–6.
[31] Hajiloo A, Xie WF. Fuzzy fractional-order PID controller design using multi-objective optimization, 2013 Joint IFSA World Congress and NAFIPS Annual Meeting (IFSA/NAFIPS), Edmonton, AB; 2013. p. 1445–1450.
[32] Ramiro SB, Manuel FS, Tenreiro Machado JA. Tuning and application of integer and fractional order pid controllers. Netherlands, Dordrechtpp: Springer; 2009. p. 245–55.
[33] Padula F, Visioli A. Tuning rules for optimal PID and fractional-order PID controllers. J Process Control 2011;21(1):69–81.
[34] Yan Zhe et al. Realization of fractional order controllers by using multiple tuning-rules. Int J Signal Process Image Process Pattern Recognit 2013;6(6):119–28.
[35] Ghosh A et al. Design and Implementation of a 2-DOF PID compensation for magnetic levitation system. ISA Trans 2014;53:1216–22.
[36] Dimeas I, Petras I, Psychalinos C. New analog implementation technique for fractional-order controller: a DC motor control. AEU – Int J Electron Commun 2017;78:192–200.
[37] Vastarouchas C, Tsirimokou G, Freeborn TJ, Psychalinos C. Emulation of an electrical-analogue of a fractional-order human respiratory mechanical impedance model using OTA topologies. AEU – Int J Electron Commun 2017;78:201–8.
[38] Magnetic Levitation: Control Experiments Feedback Instruments Limited, UK; 2011.
[39] Debnath L. Recent applications of fractional calculus to science and engineering. Int J Math Math Sci 2003;54(54):3413–42.
[40] Oustaloup A et al. Frequency band complex non integer differentiator: characterization and synthesis. IEEE Trans Circuit Syst – I: Fundam Theory Appl 2000;47(1):25–39.
[41] Das S, Pan I. Fractional order signal processing: introductory concepts and applications. Springer; 2011.
[42] Matignon D. Generalized fractional differential and difference equations: stability properties and modelling issues. In: Proc. of Math. Theory of Networks and Systems Symposium, Padova, Italy; 1998.
[43] Podlubny I. Fractional-order systems and $PI^{\lambda}D^{\mu}$ controllers. IEEE Trans Autom Control 1999;44(1):208–14.
[44] Oustaloup A. La Commande CRONE: Commande Robuste d'Ordre Non Entier. Paris: Hermes; 1991.